frontiers | Frontiers in Biomaterials Science

TYPE Original Research
PUBLISHED 20 September 2022
DOI 10.3389/fbiom.2022.925471

OPEN ACCESS

EDITED BY
Susana G. Santos,
Universidade do Porto, Portugal

REVIEWED BY
Antoniac Iulian,
Politehnica University of Bucharest, Romania
Xiao Lin,
Soochow University, China

*CORRESPONDENCE
Sandra Sefa,
sandra.sefa@hereon.de
Silvia Galli,
silvia.galli@mau.se

SPECIALTY SECTION
This article was submitted to Bio-interactions and Bio-compatibility, a section of the journal Frontiers in Biomaterials Science

RECEIVED 21 April 2022
ACCEPTED 25 August 2022
PUBLISHED 20 September 2022

CITATION
Sefa S, Wieland DCF, Helmholz H, Zeller-Plumhoff B, Wennerberg A, Moosmann J, Willumeit-Römer R and Galli S (2022), Assessing the long-term in vivo degradation behavior of magnesium alloys - a high resolution synchrotron radiation micro computed tomography study.
Front. Biomater. Sci. 1:925471.
doi: 10.3389/fbiom.2022.925471

Assessing the long-term *in vivo* degradation behavior of magnesium alloys - a high resolution synchrotron radiation micro computed tomography study

Sandra Sefa[1]*, D.C. Florian Wieland[1], Heike Helmholz[1], Berit Zeller-Plumhoff[1], Ann Wennerberg[2], Julian Moosmann[3], Regine Willumeit-Römer[1] and Silvia Galli[4]*

[1]Institute of Metallic Biomaterials, Helmholtz Zentrum Hereon, Geesthacht, Germany, [2]Institute of Odontology, University of Gothenburg, Goteborg, Sweden, [3]Institute of Materials Physics, Helmholtz Zentrum Hereon, Geesthacht, Germany, [4]Department of Prosthodontics, Faculty of Odontology, University of Malmö, Malmö, Sweden

Biodegradable magnesium (Mg) implants are emerging as a potential game changer in implant technology in situations where the implant temporarily supports the bone thereby avoiding secondary surgery for implant removal. However, the consequences of the alteration in the degradation rate to bone healing and the localization of degradation and alloying products in the long term remain unknown. In this study, we present the long-term osseointegration of three different biodegradable Mg alloys, Mg-10Gd, Mg-4Y-3RE and Mg-2Ag, which were implanted into rabbit femur for 6 and 9 months. In addition, we have investigated the effect of blood pre-incubation on the *in vivo* performance of the aforementioned alloys. Using high-resolution synchrotron radiation based micro computed tomography, the bone implant contact (BIC), bone volume fraction (BV/TV) and implant morphology were studied. The elemental traces have been characterized using micro X-ray fluorescence. Qualitative histological evaluation of the surrounding bone was also performed. Matured bone formed around all three implant types and Ca as well as P which represent parts of the degradation layer were in intimate contact with the bone. Blood pre-incubation prior to implantation significantly improved BIC in Mg-2Ag screws at 9 months. Despite different implant degradation morphologies pointing toward different degradation dynamics, Mg-10Gd, Mg-4Y-3RE and Mg-2Ag induced a similar long-term bone response based on our quantified parameters. Importantly, RE elements Gd and Y used in the alloys remained at the implantation site implying that they might be released later on or might persist in the implantation site forever. As the bone formation was not disturbed by their presence, it might be concluded that Gd and Y are non-deleterious. Consequently, we have shown that short and mid-term *in vivo* evaluations do not fully represent indicators for long-term osseointegration of Mg-based implants.

KEYWORDS

biodegradable implants, magnesium-based implants, degradation products, synchrotron radiation micro-computed tomography, micro X-ray fluorescence, bone healing

1 Introduction

Biodegradable magnesium (Mg)-based implants are of great interest in musculoskeletal research and application due to their ability to degrade in the body, thus requiring no secondary surgery for removal in situations where the implant is not meant to remain in the body permanently (1–4). Apart from their degradability, the Young's modulus of Mg is similar to that of bone and hence causes less stress shielding compared to conventional implant materials such as titanium (Ti) and medical steel (5). Mg occurs naturally in the human body and enhances cellular processes (6,7). However, it can degrade rapidly and might not allow bone sufficient time to heal before it is fully degraded. Upon degradation, Mg yields corrosion products that can be excreted or integrated into the natural metabolic process depending on their release rate (8) and the biological processes occurring in its environment (9,10). The local increase in pH and the release of hydrogen gas during degradation can compromise the integration of the implant and, thus, its ability to support bone healing with an associated risk of tissue necrosis leading to delayed or no healing (11).

Existing solutions to improve Mg performance focus on either surface modification techniques or changing the composition, which results in a change in the microstructure. With a focus on microstructure modifications, suitable elements such as Aluminum (Al), Manganese (Mn), Calcium (Ca), Zinc (Zn), Silver (Ag), Gadolinium (Gd), Yttrium (Y), and several other rare earth (RE) elements are used to dope pure Mg to improve its mechanical and physical properties (12). In this regard, the addition of 10 weight percent (wt%) of Gd to form Mg-10Gd or 2 wt% of Ag to form Mg-2Ag or 4 wt% of Y, 2 wt% of Nd, 1 wt% of Ce to form Mg-4Y-3RE respectively improves the corrosion resistance and mechanical properties of Mg (13). Additionally, coatings such as calcium phosphate (CaP) and degradable polymers such as nanostructured hydroxyapatite (nHA) can be applied to Mg alloys to change the surface chemistry in order to minimize the corrosion rate to the level tolerable by the body as well as to improve cell adhesion (14). Alternatively, adhesion of proteins to Mg alloys is known to improve their performance. An example is harnessing the natural protective layer formed around Mg alloys when they come into contact with body fluids such as blood, thereby reducing the corrosion rate (14). Willumeit et al. showed that the pre-incubation of Mg alloys under cell culture conditions improves their tissue compatibility (15). Zhang et al. has also demonstrated that Mg^{2+} ions exhibited high binding to bovine serum albumin (BSA) due to the attraction between the negatively charged oxygen ions and the Mg^{2+} ions (16) generated during degradation. The first event that occurs after the implantation of a biomaterial is the adsorption of proteins on its surface upon contact with blood (17). The adsorbed proteins (18) majorly determine a cascade of biological responses and the material biocompatibility (17) by shaping the crucial characteristics of cellular response such as adhesion, spreading, migration, proliferation and differentiation (19,20). Some *in vitro* studies have shown that protein coatings are known to offer a natural protective layer to Mg alloys by decreasing the corrosion rate and improving cell adhesion and, consequently biocompatibility (15,21). Yamamoto et al. further reported that adsorbed proteins form insoluble salts with degradation products that mitigate the rapid degradation of pure Mg (22). Moreover, the modulation of hydrogen evolution in Mg degradation by protein as well as the reduction in corrosion suseptibility when albumin (the most abundant blood protein) is added to simulated body fluid is reported (23). It is postulated that, proteins can alter the topology and chemical property of Mg alloys thus affecting the degradation behavior of Mg remarkably (24). A blood-contact experiment for Mg alloys has revealed differences in corrosion layer composition among the different Mg alloys when in contact with blood (25). It has also been reported elsewhere that Ti implants with calcium-ion modified surfaces, when in contact with blood, improve their coagulatory effect and subsequently yield a better biological response (18). Owing to the fact that the adsorption of proteins on the surface of Mg alloys significantly affects its biological outcome (15) and offers protective benefits against rapid corrosion (25) therefore, the translational potential of pre-incubating Mg alloys with blood prior to implantation is to offer protection against rapid corrosion by the formation of a first corrosion layer and also increase its osteogenic potential which might then translate into better osseointegration in *in vivo* applications.

Witte et al. showed that the *in vivo* degradation mechanisms and bone response of Mg-alloys depend on their elemental composition. The corrosion products usually formed are biological phosphate constituents (27). Jähn et al. compared the degradation of Mg-2Ag pins under *in vitro* and *in vivo* conditions and found that Mg-2Ag enhanced bone formation and did not cause systemic adverse effects. Furthermore, Mg-2Ag improved the osteoblast activity and differentiation but had the opposite effect on osteoclasts leading to the formation of augmented callus during fracture healing (28). The addition of diluted forms of Ag is known to combat bacterial infection (29). On the other hand, Galli et al. reported a poor osseointegration performance of Mg-2Ag *in vivo* as having an inadequate contact with bone amidst fibrous tissue encapsulation after 1 month of

implantation (13). Another extensively studied Mg alloy is Mg-10Gd. Gd is a RE element that has raised concerns about possible cytotoxicity although it is already used as a contrast agent in medicine. In one of our recent studies, Krüger et al. reported that Mg-10Gd alloys released Gd ions that were below the toxicity level in cell culture. It was further reported that Mg-10Gd alloys form a stable degradation layer surrounded by new bone tissue (30). Also, in a study by Myrissa et al., the toxicity associated with Mg-10Gd was investigated and it was concluded that there was no increase in Mg or Gd concentration in blood serum samples even after 36 weeks of implantation (31). Additionally, *in vitro* experiments (32,33) have reported that Gd is below the toxicity level in cell culture with improved osteoblastic mineralization (34). Mg-4Y-3RE alloys are a member of the WE systems known to have good mechanical properties and suitable degradation rates (35). Some variations of this composition are already in clinical applications. An example is MAGNEZIX compression screw which has been shown to be clinically equivalent to Ti screws in the treatment of hallux valgus (36). Both Mg-10Gd and Mg-4Y-3RE alloys have been shown to have a good osteogenic effect on bone after 3 months observation period as opposed to Mg-2Ag having a poor osteogenic response (13).

So far, the long-term *in vivo* evaluation of the degradation of Mg-based implants as well as the influence of blood pre-incubation on their *in vivo* performance have not been studied using high resolution using synchrotron radiation x-ray computed tomography (SRμCT) at long healing times (6 and 9 months). Studying the bone response of Mg-based implants with the use of SRμCT yields greatly enhanced image quality that reveal subtle differences among the alloys through improved signal-to-noise ratio. Furthermore, SRμCT enables the study of the morphology of the degraded screws and the surrounding bone non-destructively in 3D at a resolution of less than 1 μm (37). The added knowledge gained from *in vivo* evaluation of Mg-based implants in the long-term will continue to expedite the use of Mg-based implants in clinical applications.

In the current work, our first aim is to investigate the osseointegration of two binary biodegradable Mg alloys (Mg-10Gd and Mg-2Ag) against a ternary biodegradable Mg alloy (Mg-4Y-3RE) in order to gain deeper insight into which alloying element better improves the *in vivo* performance of Mg in the long term. Secondly, we aim to investigate if the pre-incubation of the Mg alloys in blood prior to implantation improves their osseointegration. The outcome of these investigations will add to the existing knowledge to guide the selection of alloying elements that better improve the osseointegration of Mg alloys in the long term. Also, this study will enable us to understand if early adsorption of proteins unto the surfaces of Mg alloys offers additional benefits by favorably modulating osteogenic cellular behavior. As Mg degrades, its mechanical integrity is continuously changing, which might affect its mechanical competence over an extended period of time. Thus, long-term studies can enable the monitoring of the effect of Mg degradation on bone healing throughout its lifetime until it is fully degraded. In this regard, the following research questions are addressed: (I) Does bone apposition differ among the types of Mg-based screws at longer healing times? (II) Does Mg degradation compromise bone implant contact (BIC) at longer healing times? (III) Does the blood pre-incubation of the screws prior to implantation affect their osteogenic response? In view of this, the aim of the study is to compare the long-term *in vivo* performance of Mg-2Ag, Mg-10Gd and Mg-4Y-3RE screws by quantifying the bone formation and integrity of the contact at the bone implant interface as well as to characterize the constituent of their degradation products at 6 and 9 months implantation times. In addition, the effect of blood pre-incubation on the *in vivo* performance of the screw is studied. To this end, we utilized SRμCT, micro X-ray fluorescence spectroscopy (μXRF) and histomorphometry techniques to provide an in-depth assessment of bone response to the aforementioned Mg-based alloys. μXRF enables the determination of the spatial distribution of the constituent elements in each alloy. Histomorphometry can reveal mineralized and cellular components as well as subtle patterns regarding peri-implant bone healing. Thus, the combined information from all three modalities will yield in-depth knowledge on Mg-based implants and bone interaction in the long term. It is hypothesized that the three selected Mg alloys should induce a similar bone healing response with good anchorage in the surrounding bone over the observation period.

2 Materials and methods

The implant screws were produced at Helmholtz Zentrum Hereon Magnesium Innovation Centre (Hereon MagIC, Germany). In the first step of the production, the starting materials: magnesium (99.99%, Xinxiang Jiuli Magnesium Co. Ltd., China), yttrium (Y, 99.95%, Grirem Adv. Mater. Co. Ltd, China), gadolinium (Gd, 99.95%, Grirem Adv. Mater. Co. Ltd, China), a rare earth mixture, (RE, Grirem Adv. Mater. Co. Ltd, China) and silver (Ag, 99.99% ESG Edelmetall-Handel GmbH & Co. KG, Germany) were used to cast the Mg alloys in this study based on permanent mold gravity casting technique. Ag in Mg-2Ag, Gd in Mg-10Gd, Y and RE mixture in Mg-4Y-3RE were heated and added to melted (720°C) pure Mg and stirred continuously for 15 min. Using boron-nitride (BN) as mold release agent, the mixture was poured into a pre-heated (550°C) permanent steel mold. Casting was performed in a controlled atmosphere with 2 wt% sulfur hexafluoride (SF_6) followed by solution heat treatment (T4) of the alloys for 6 h at 430°C (Mg-2Ag) or 550°C (Mg-10Gd and Mg-4Y-3RE) to refine the grain size. The billets obtained were then extruded. All the screw types were extruded using the indirect method. Mg-2Ag screws were extruded at a temperature of 300°C with a speed of 2 mm/s. For Mg-10Gd, extrusion was performed at 430°C with a speed of 3.5 mm/s while Mg-4Y-3RE was extruded with a speed

of 3 mm/s and at a temperature of 360°C. The screws were subsequently refined to obtain threaded mini screws with 2 mm outer diameter and 2 mm length. The screws were placed in sealed plastic envelopes followed by gamma sterilization (dose of 27 kGy at BBF, Sterilization service, Kersen, Germany).

2.1 Measurement of initial screw volumes

The initial volumes of the screws were measured as a reference value. For this, three screws per type of material were scanned before implantation using a Phoenix Nanotom benchtop µCT (GE inspection and sensing technologies, Wunstorf, Germany) at an operating voltage of 100 kV and a current of 70 µA. The exposure time and the number of projections were 1000 ms and 2700 projections, respectively. The binned voxel size was 2.5 µm. The image data was thresholded prior to the volume calculations using an open-source image processing software, Fiji (Fiji is just ImageJ, GPL v2) (38,39). Using the voxel counter plugin, the volume of the screws was calculated by summing the foreground voxels. The summed voxels were converted to mm^3 by multiplying with the voxel size cubed.

2.2 Animal study

The *in vivo* study was approved by the ethical committee of the French Ministry of Higher Education and Research (approval number 00391-01) and performed at the National School of Veterinary Medicine of Maison-Alfort (Maison-Alfort, France). Six mature female New-Zealand white rabbits were used for the study (weight 3–4 kg). The animals were put on general anesthesia with intramuscular administration of the following drugs: 250 mg/kg of medetomidine (Domitor, Zoetis, France), 20 mg/kg ketamine (Imalgene 1000, Merial, Sanofi, France) and 1 mg/kg of diazepam (Valium, Roche, France). Immediately after anesthesia, a few mL of blood was collected from each rabbit and three Mg screws, one per material, were incubated in the blood of the same rabbit they were about to be inserted for half an hour. The blood was added directly in the sterilized container of each screw in the pre-incubation group and immediately removed and implanted after half an hour. Local anesthesia was administered with 1 mg lidocaine injected into the surgical area. A full thickness incision of skin and muscles was made in the hindlimb, in the region of the distal femoral metaphysis. The periosteum was elevated and the bone in the diaphysis of the femur, next to the distal femoral metaphysis, was exposed. Three osteotomies were performed in this region with a rotating drill under irrigation with sterile saline. The drill sequence was as follows: round bur, diameter 1.4 mm, parallel bur, 2 mm, tapping with a Ti instrument with the same threaded shape of the Mg screws. Thereafter, three Mg-screws (one material each) were inserted with a manual screwdriver in the osteotomies. In one leg, pristine screws were implanted, while in the other leg, screws pre-incubated in blood for 30 min were implanted (randomly allocation of right or left leg). In total, 36 screws were inserted in the six animals. The screws were inserted flush to the bone and with 5 mm bone between the next screw (Figure 1). The periosteum, muscle and skin were repositioned and sutured with a resorbable suture in 2 layers (Vicryl 3.0). The rabbits were housed in separate cages and allowed to move freely and eat and drink *ad libitum*. They also received antibiotics and analgesic therapy for 5 days post-surgery. After 6 and 9 months of implantation, the rabbits were euthanized (three rabbits per time point) with a lethal dose of sodium pentobarbital (Euthasol, Virbac, Fort Worth, United States). The legs were dissected to expose the bone around the implantation site. The screws with the surrounding bone were explanted using a cylindrical trephine bur of 3.4 mm diameter. The bone-implant blocks (explants) were fixed in 70% ethanol for approximately 1 day and were then dehydrated in ethanol followed by critical point drying to halt the Mg degradation and preserve the bone tissue morphology.

2.3 Synchrotron radiation x-ray computed tomography data acquisition and analysis

All six rabbits survived throughout the observation period and were all scanned using SRµCT. For a quantitative assessment of osseointegration, the volume of the degradation layers, BIC and BV/TV were calculated from the SRµCT image data. The degradation rate was not calculated because it was not possible to distinguish between the degradation layer and the residual screw. Nevertheless, the volume of the "remnant screws" were calculated based on the SRµCT data. Where remnant screw refers to the undistinguished residual screw and the degradation layer. Based on the calculated volumes together with the appearances of the remnant screws, qualitative evaluation was inferred regarding the degradation rates of the three Mg screws.

2.3.1 Synchrotron radiation x-ray computed tomography image data acquisition

Imaging of the explants was conducted at the P05 imaging beamline IBL operated by Helmholtz-Zentrum Hereon at the PETRA III storage ring at the Deutsches Elektronen Synchrotron (DESY), Hamburg Germany (40–43). The imaging was performed in two batches during two different beamtimes. The first batch of data consisted of 24 samples. For each sample in this batch, 2400 projections over a total angle

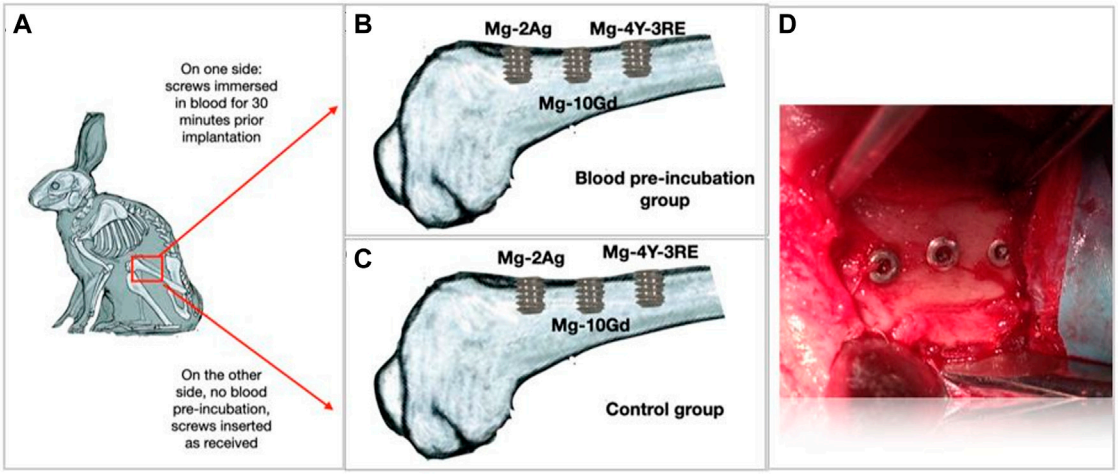

FIGURE 1
Schematic figure of the implanted screws in the rabbit femur. **(A–C)** Schematic figure of the insertion of the screws in the rabbit femur. Each rabbit received three blood pre-incubated screws, one per material, on one leg and three screws without blood pre-incubation, one per material, on the other leg, for a total of 6 screws per rabbit (36 screws in the entire study). **(D)** A photo of three screws in one rabbit femur.

of 360° at an energy of 45.33 keV were recorded. A 3D image volume with a binned effective voxel size of 2.56 µm was reconstructed using a filtered back projection algorithm (44). The second batch of data consisted of 12 samples. For each sample in this batch, 4800 projections over a total angle of 360° at an energy of 51.50 keV were recorded. A 3D image volume with a binned effective voxel size of 3.84 µm was reconstructed using a filtered back projection algorithm (44).

2.3.2 Image pre-processing, segmentation, registration and resampling

To decrease the computational effort due to the high resolution of the image data, all image data were pre-processed to reduce their size. For this task, Fiji/ImageJ was used. First, the reconstructed data were isotropically binned with a factor of two, then the bit depth was reduced from 32 bit to 16 bit within a range of −0.004 and +0.02 resulting in 5.12 µm voxel size for the first batch and 7.68 µm for the second batch respectively. The data set were then filtered using an iterative nonlocal means denoising filter (45). The first batch of data was resampled to 7.68 µm to have all the data with the same voxel size for further analysis. The image data were segmented semi-automatically using the WEKA segmentation plugin in Fiji/ImageJ with subsequent manual corrections. After segmentation of the tomograms, the image data were registered and resampled to a custom-made orientation cylinder as a pre-requisite for the quantitative analysis. Subsequently, the volume of the degradation layers of the screws were calculated in Avizo (version 9.4.2, Thermo Fisher Scientific, Waltham, MA).

2.3.3 Image analysis of the synchrotron radiation x-ray computed tomography data

The parameters BV/TV and BIC were all calculated over the entire volume (3D) of the tomograms within 300 µm volume of interest (VOI) around the screws using a custom-written Fiji script. The VOI analyzed represents the region in the screw thread and the thread tips.

2.3.3.1 Bone to implant contact and bone volume fraction

To evaluate osseointegration, the BIC was calculated. BIC is the area of the screw (degradation layer) in contact with the surrounding bone. To calculate the normalized BIC, Eq. 1 is used. To evaluate the effect of the screws on the surrounding bone, BV/TV was calculated as the ratio of mineralized bone (BV) over the entire volume of tissues (TV) in the VOI using Eq. 2. The details of the 3D calculations are found elsewhere (30,46). The degradation rate was not calculated because there was no clear contrast between the degradation layer and the residual screw.

$$3D - BIC\ [\%] = \frac{\#\ surface\ voxels\ of\ implant\ in\ contact\ with\ bone}{\#total\ surface\ voxels\ of\ screw} \quad (1)$$

$$3D - \frac{BV}{TV}\ [\%] = \frac{\#\ voxels\ of\ bone\ volume}{\#\ voxels\ of\ total\ volume\ of\ the\ VOI} \quad (2)$$

2.3.4 Histology

Histological analyses were performed to qualitatively assess bone response to the Mg screws. The same samples used in the

SRμCT measurement were infiltrated with absolute ethanol for a week followed by infiltration with a methyl-methacrylate based resin by LLS Rowiak Laser Lab Solutions GmbH (Hanover, Germany). Forty-μm sections were cut along the longitudinal axis of the screw based on cutting-grinding technique proposed by Donath (47) using an Exakt system (Exakt Apparatebau, Nordertedt, Germany). The sections were stained with toluidine blue (Histlab, Göteborg, Sweden) and imaged with an optical light microscope (Eclipse ME600, Nikon, Tokyo, Japan).

2.3.5 Micro X-ray fluorescence spectroscopy

Elemental mapping of the degradation products of the screws at 9 months degradation time was performed with a Tornado M4 μXRF spectrophotometer (Bruker Nano, Berlin, Germany) set up with a rhodium (Rh) tube and tungsten (W) tube at a working voltage of 50 kV and anodic current of 600 μA. A Bruker XFlash ® Silicon Drift Detector detects the fluorescence signal with an energy resolution of <145 eV for 250 cps. The measurement was performed under vacuum conditions (20 mbar) using a beam spot size of 25 μm and a beam spot distance of 25 μm with an acquisition time of 1.5 ms per pixel. To obtain high resolution images, image acquisition was performed with 3 cycle runs. Data acquisition and processing was performed with the Bruker ESPRIT microanalysis software version 1.3.0.3273.

2.3.6 Statistical analysis

All statistical analysis were performed in Origin 2021b. The mean and standard deviation of all analyzed parameters were calculated for each screw type per time point. The group means were compared using one-way analysis of variance (ANOVA) with Tukey´s multiple comparison test assuming a normal distribution. In addition, a paired t-test was performed on the blood pre-incubated screws and control screws to investigate the effect of blood pre-incubating of the screws on the BV/TV and BIC for each screw type and at each implantation time. The parameters were compared between the alloy types at the implantation times (6 and 9 months). All analysis was performed at 95% confidence interval, thus, a p-value below 0.05 was considered statistically significant.

3 Results

3.1 Qualitative evaluation of magnesium implant integration

3.1.1 Tissue integration and qualitative evaluation of screw degradation

All screw types were altered in their original shape and density. In Figure 2, 2D SRμCT slices of each screw type after 6 and 9 months of implantation show that Mg-10Gd and Mg-4Y-3RE had retained the original threaded screw shape, whereas Mg-2Ag had a distorted shape. This observation is also corroborated by the 3D rendering of the screws shown in Figure 3. Interestingly, even though the degradation products of Mg-2Ag appear to be severely disintegrated, they remained attached to the bone, as seen in the inset of Figure 2. The x-ray absorption coefficient between the degradation layer and residual screw was similar and could not be distinguished in the SRμCT image data (Figure 2) thus, the degradation rate could not be calculated. Nonetheless, representative 2D histological slides show that almost all the original metal had transformed in degradation products. For Mg-10Gd and Mg-4Y-3RE the degradation products remained attached to the original metal, maintaining the original threaded shape. For Mg-2Ag, part of the degradation layers was still attached to a core of residual original metal, but had not maintained the same original shape. For all three materials, a core of residual screws was visible at 6 months in the histologies (Figure 4, red arrows). The histological slides further reveal that the metallic residue in Mg-10Gd (Figure 4) and Mg-4Y-3RE (Figure 4) have a similar dark appearance compared to Mg-2Ag (Figure 4), which appeared dark brown. The SRμCT slice of Mg-10Gd (Figure 2) and Mg-4Y-3RE (Figure 2) show the presence of high intensity structures. These high intensity structures seen in Mg-4Y-3RE can also be observed in their corresponding histological data (Figure 4) but in the case of Mg-10Gd, the high intensity areas are not noticeable in their corresponding histological data (Figure 4). The insets in (Figures 2, 4) both highlight the bonding between the degradation layer and the bone of all screw types.

From our observations, the bone tissue response to the Mg screws appeared similar at both implantation times. At the end of the two implantation times (6 and 9 months) and for all screw types, the osteotomy gap had been completely bridged and the screws were fully integrated into the surrounding bone. Figures 2, 4 show the intimate contact among all the screw types with the bone environs. All screw types appear to be surrounded by healthy bone due to the presence of osteocytes in the bone around the screws (Figure 4).

3.1.2 Characterization of degradation products

Figure 5 shows representative constituent maps of the three Mg alloy types that were characterized using μXRF at 9 months implantation time. Small amount of residual metal was present in all screw types which can be deduced from the map showing the distribution of Mg. Therefore, it is obvious that the other part of the screw has turned into degradation layer. The degradation products of Mg-10Gd and Mg-4Y-3RE maintained their original screw shapes while the degradation products of Mg-2Ag appear distorted. As expected, Gd signal was detected in Mg-10Gd alloys. The alloy Mg-4Y-3RE clearly showed a Y signal in the degradation layer while Mg-2Ag had silver (Ag) signal in the degradation layer. Calcium (Ca) and phosphorus (P) signals were detected in the degradation layer of all screw types. Also, for

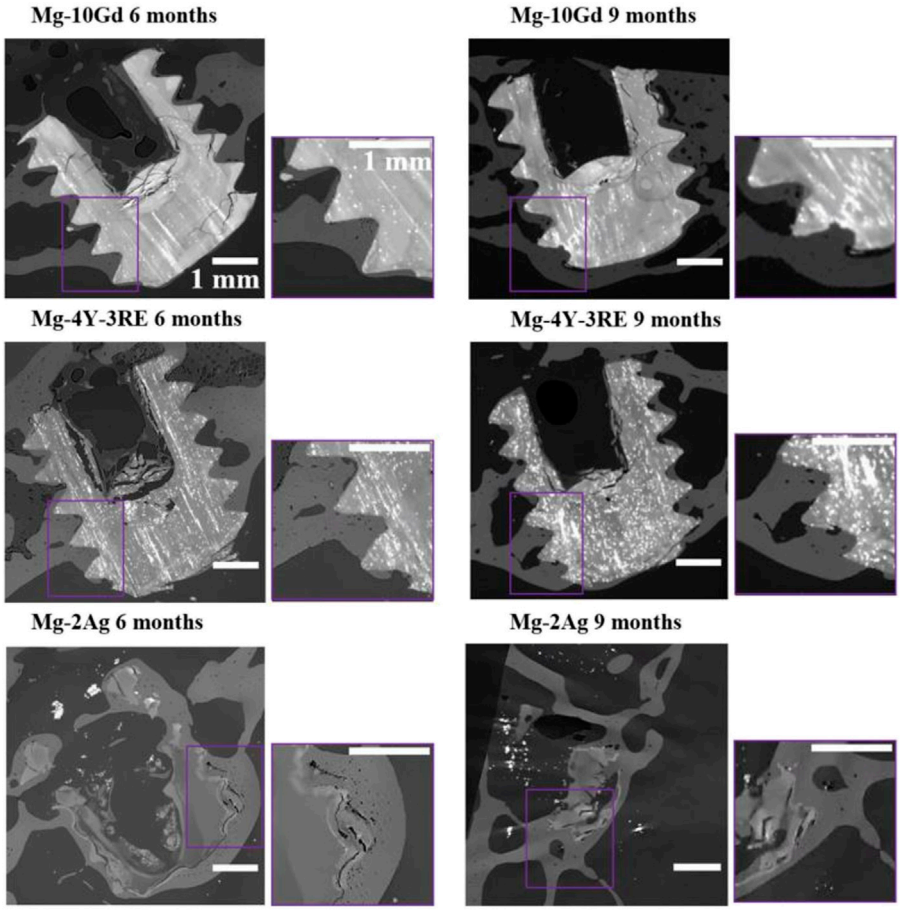

FIGURE 2
2D longitudinal slices of a SRμCT scan of three Mg-based screws after 6 and 9 months of implantation showing the encapsulation among all the screw types in the surrounding bone. The image shows good osseointegration involving all the screw types. The insets highlight the bonding between the degradation layer and bone of all screw types. Notably, Mg-2Ag bonded to the bone despite severe disintegration.

all screw types, sulfur (S) signals were detected in the degradation layer and surrounding soft tissue. The enrichment of S at the site of Mg-2Ag implant indicates the strong association of proteins to Ag (48,49).

3.2 Quantitative evaluation of magnesium screws integration

The quantitative evaluation of osseointegration was based on the SRμCT image data. The evaluated parameters are all presented in Figure 6 as box plots.

3.2.1 Bone volume fraction in the vicinity of Mg-10Gd, Mg-4Y-3RE and Mg-2Ag screws

The results of BV/TV within a VOI of 300 μm which is the region within the screw threads and tips are presented in Figure 6A. At 6 months, all the 3 screw types yielded a BV/TV above 40%, with Mg-10Gd (47.92 ± 7.31%) having the highest mean BV/TV followed by Mg-4Y-3RE (46.81 ± 9.95%) while Mg-2Ag (42.22 ± 18.08%) had the least mean BT/TV. The differences in the mean values were not significant among the screws ($p > 0.05$). At 9 months, there was a change in the order of BV/TV among the screw types. Mg-4Y-3RE (43.57% ± 13.62) had the highest mean BV/TV followed by Mg-2Ag (40.33 ± 0.11%) while Mg-10Gd (31.12 ± 15.77%) had the least mean BT/TV. The differences in the mean values did not reach the level of significance ($p > 0.05$).

3.2.2 Effect of blood pre-incubation of magnesium alloys on bone volume fraction

Figure 7A show the effect of blood pre-incubation of the screws in blood freshly obtained from the rabbits prior to implantation on BV/TV over time. Generally, the control group had higher average BV/TV compared to the blood pre-incubated group of all screws at both 6 and 9 months. At

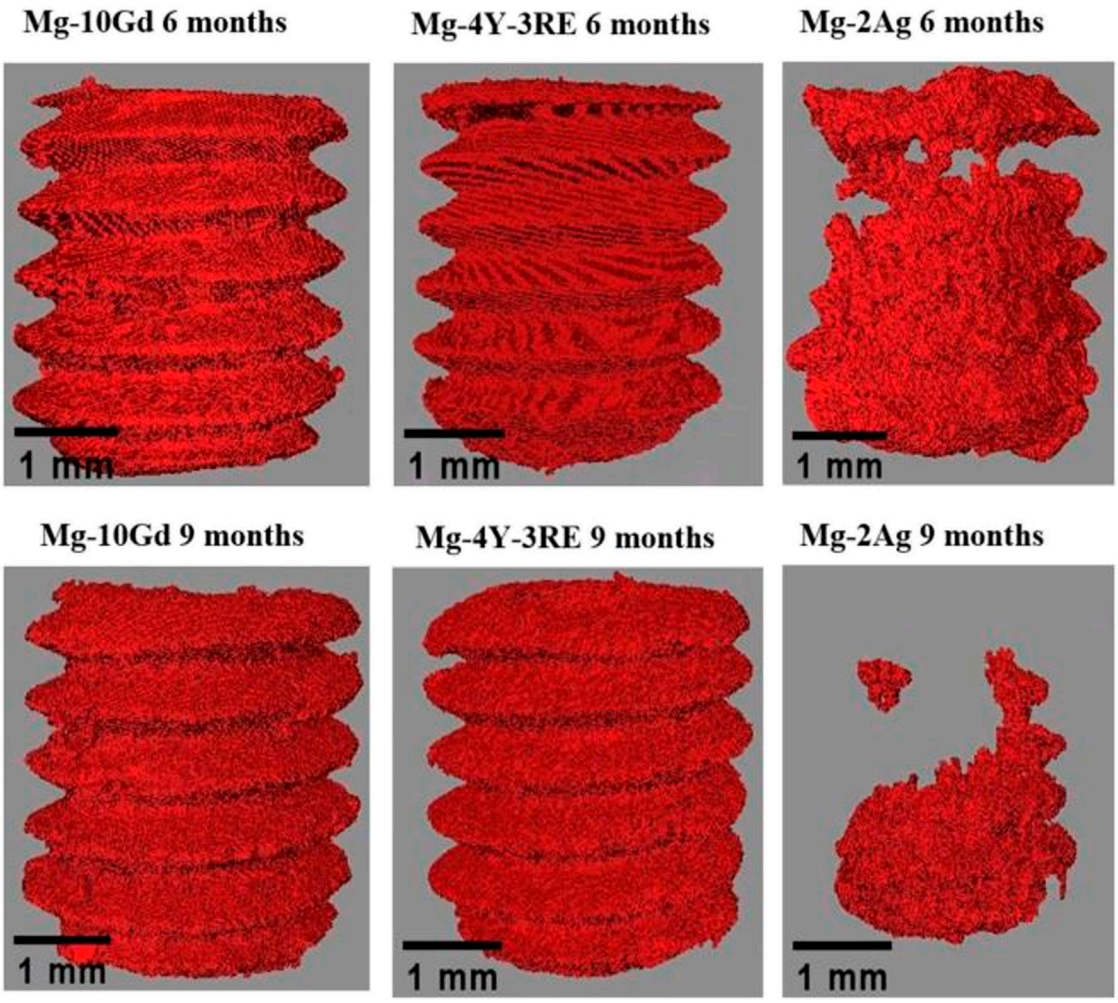

FIGURE 3
3D rendering of a SRμCT scan of three Mg-based screws showing their appearance after 6- and 9-months implantation time. The image shows visible alteration in the geometry of Mg-2Ag whereas the Mg-10Gd and Mg-4Y-3RE maintained the original threaded screw shape after degradation.

6 months, the average BV/TV of blood pre-incubated Mg-2Ag group (30.82 ± 17.39%) was significantly (p = 0.04) lower than the average BV/TV of the control Mg-2Ag group (53.62 ± 11.19%). Also, at 9 months, the blood pre-incubated Mg-2Ag group (33.34 ± 4.4%) had non-significantly (p = 0.21) lower average BV/TV compared to the control group (47.23 ± 10.34%). For Mg-10Gd, the blood pre-incubated group (44.54 ± 1.72%) had non-significantly (p = 0.41) lower average BV/TV compared to the control Mg-10Gd group (51.29 ± 9.83%) at 6 months. In the same way, the blood pre-incubated Mg-10Gd group (27.87 ± 5.53%) had non-significantly (p = 0.94) lower average BV/TV compared to the control group (29.28 ± 24.32%) at 9 months. Similarly, blood pre-incubated Mg-4Y-3RE group (46.17 ± 5.15%) had slightly non-significant (p = 0.92) lower average BV/TV compared to the control Mg-4Y-3RE group (47.44 ± 14.82%) at 6 months and at 9 months, the blood pre-incubated Mg-4Y-3RE group (42.41 ± 5.11%) had non-significantly (p = 0.88) lower BV/TV compared to the control Mg-4Y-3RE group (44.41 ± 5.11%).

3.2.3 Bone implant contact between Mg-10Gd, Mg-4Y-3RE and Mg-2Ag screws and the surrounding bone

The results of BIC within a VOI of 300 μm around the screws are presented in Figure 6B. At 6 months, Mg-10Gd (57.60 ± 12.21%) had the highest mean BIC followed by Mg-2Ag (49.30 ± 13.55%) while Mg-4Y-3RE (44.49 ± 15.71%) had the least mean BIC. The differences in mean BIC among the screw types were not significant ($p > 0.05$). At 9 months, the mean BIC for all screw types was above 50% with Mg-2Ag (55.97 ± 15.93%) having the highest BIC followed by Mg-10Gd (54.75 ± 16.28%) while Mg-4Y-3RE (51.73 ± 11.48%) had the smallest BIC. Again, the

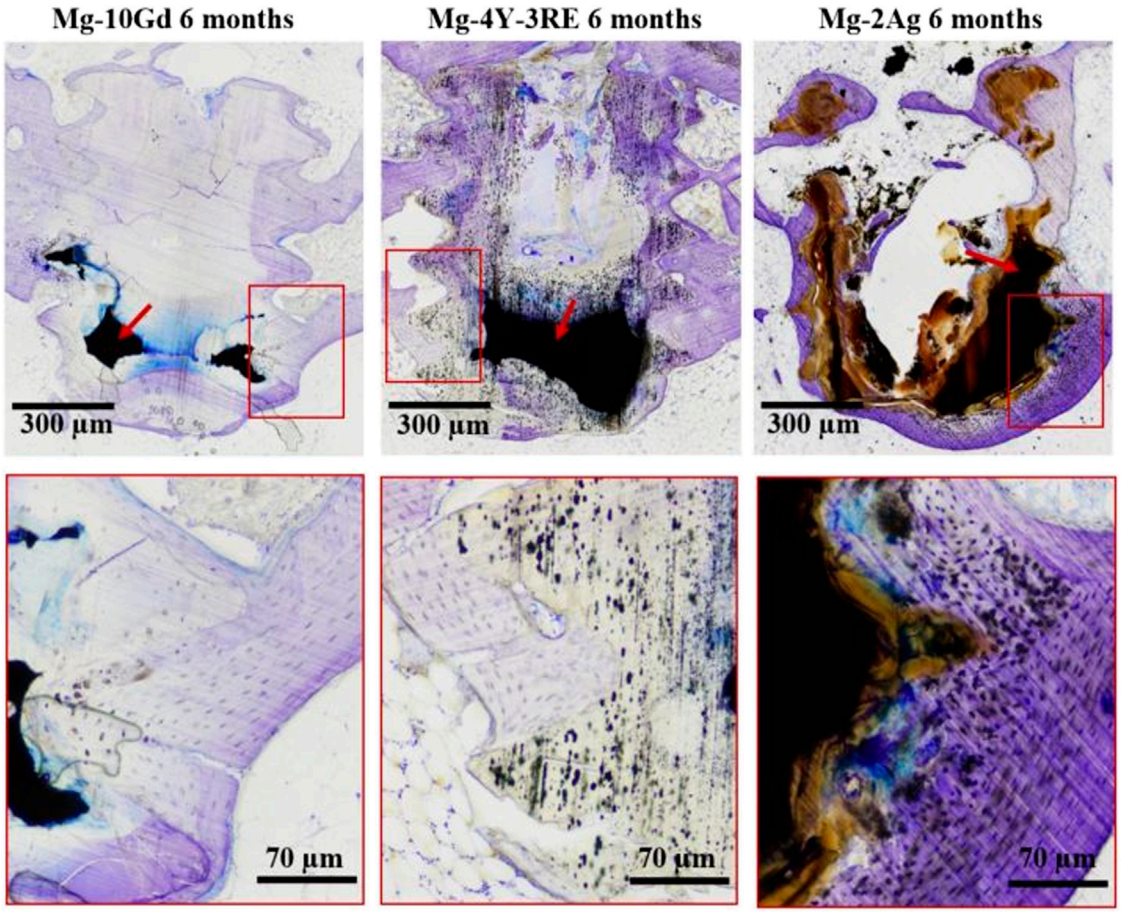

FIGURE 4
2D histological slides of Mg-10Gd, Mg-4Y-3RE and Mg-2Ag stained with toluidine blue after 6 months of implantation. Residual metal (red arrows) shown as black areas can be seen for all screw types.

differences in mean BIC were not significant ($p > 0.05$) among all the screw types.

3.2.4 Effect of blood pre-incubation of magnesium alloys on bone implant contact

In Figure 7B, the result of pre-incubating the screws with blood on BIC over time is displayed. Overall, at 9 months the mean BIC among the blood pre-incubated group was higher than the control group for all screw types except Mg-4Y-3RE which almost remained unchanged relative to the control group. At 6 months, the mean BIC of blood pre-incubated Mg-2Ag was (53.90 ± 17.52%) while that of the control group was (44.70 ± 9.41%). The average BIC was not significant ($p = 0.61$) among the two groups. However, at 9 months, the blood pre-incubated group had significantly ($p < 0.05$) higher BIC (69.53 ± 6.54%) compared to the control group (42.40 ± 6.28%). For Mg-10Gd screws, the blood pre-incubated group had slightly non-significant ($p = 0.97$) higher mean BIC (57. 81 ± 19.03%) compared to the control (57.39 ± 3.23%) at 6 months. Similarly, at 9 months the blood pre-incubated Mg-10Gd group had non-significantly ($p = 0.75$) higher BIC (52.76 ± 20.58%) than the control group (44.66 ± 17.16%). However, at 6 months, lower mean BIC was recorded for coated Mg-4Y-3RE blood pre-incubated group (35.51 ± 15.49%) compared to the control group (53.46 ± 11.64%). The difference between the mean values was not significant ($p = 0.24$). At 9 months the mean BIC was almost similar between the blood pre-incubated Mg-4Y-3RE group (51.61 ± 14.57%) and the control group (51.86 ± 10.83%). There was no statistically significant difference between the two groups ($p = 0.99$).

3.2.5 Volume of degradation layer

In Figure 6C, the result of the 3D volume analysis is displayed. The volumes of the remnant screws generally decreased over time except for Mg-4Y-3RE screws which remained almost steady over time. At 6 months, Mg-2Ag

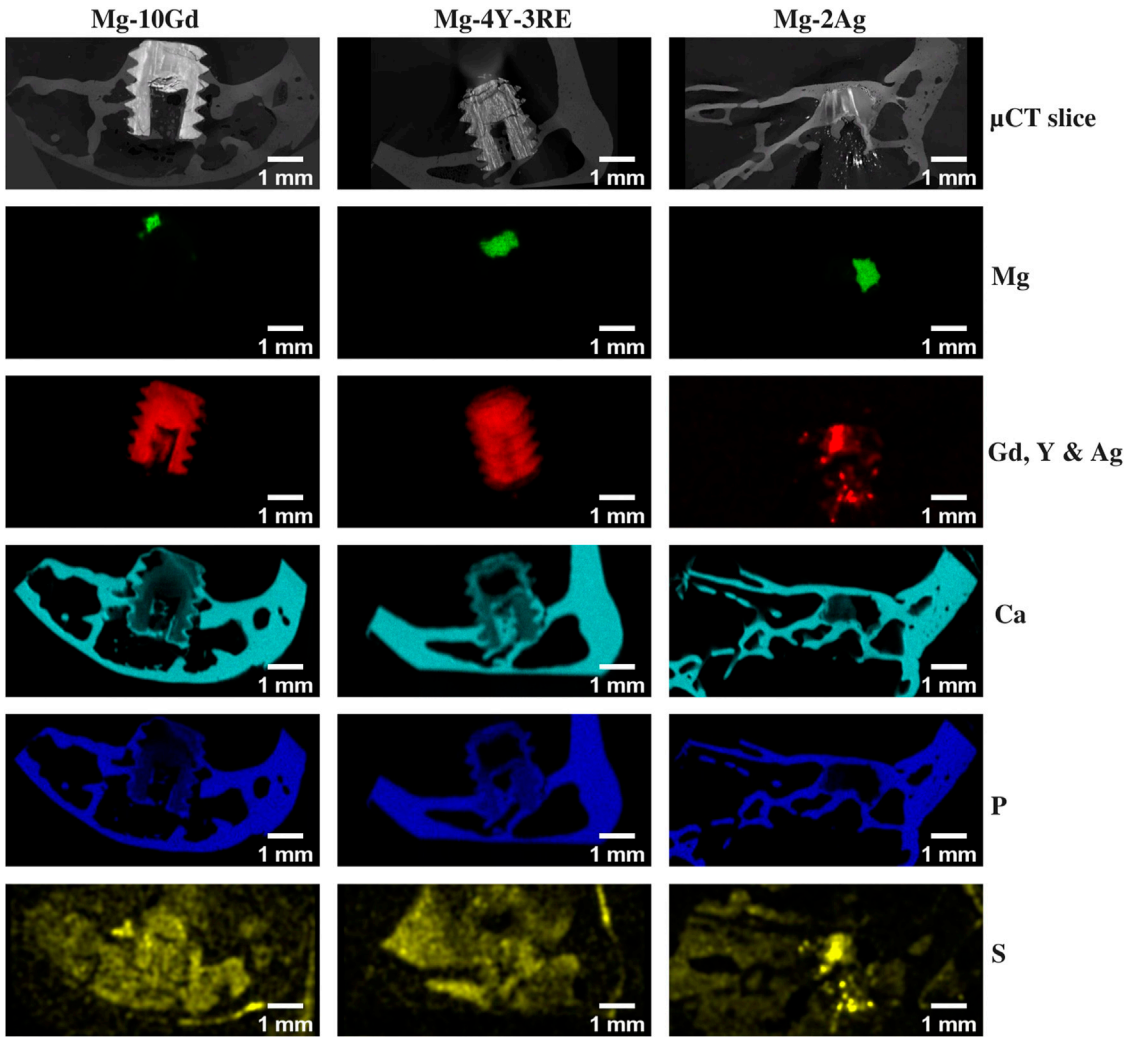

FIGURE 5
Exemplary µXRF maps of Mg-10Gd, Mg-4R-3RE and Mg-2Ag screws after 9 months of implantation.

(2.33 ± 0.55 mm^3) displayed a significantly smaller ($p < 0.05$) mean volume compared to Mg-4Y-3RE (4.84 ± 0.33 mm^3) and Mg-10Gd (4.70 ± 0.20 mm^3). The same trend was seen at 9 months, where Mg-2Ag (1.40 ± 0.55 mm^3) still had a significantly ($p < 0.05$) smaller mean volume compared to Mg-4Y-3RE (4.90 ± 0.28 mm^3) and Mg-10Gd (4.56 ± 0.46 mm^3). The initial screw volumes of all screw types are included in the boxplot (Figure 6C).

4 Discussion

Based on our applied analytical methods to evaluate the long-term bone response to binary and ternary Mg-based implants, the bone tissue reacted similarly to all screw types at both implantation times. The disintegration of Mg-2Ag precipitated bright spots, which could be assumed as Ag-oxides (13) (Figure 2). Also, high X-ray absorbing areas, which are probably GdH_2, were seen in Mg-10Gd degradation products (13) (Figure 2). It is also probable that the bright spots in Mg-4Y-3RE degradation products are Nd and Y precipitates (13) (Figures 2, 4). Intermittent micro cracks were seen in Mg-10Gd and Mg-4Y-3RE degradation products, which could be indicative of brittleness caused by repetitive loading over the course of their implantation. A considerable amount of bone surrounded the screws at both implantation times (Figures 2, 4). The average BV/TV at 6 months was above 40% for all screw types and remained almost steady for Mg-4Y-3RE and Mg-2Ag at 9 months but slightly decreased for Mg-10Gd. In our previous short and mid-term study, Galli et al. has reported fibrous tissue encapsulation around Mg-2Ag at 1 month and observed unmineralized bone around Mg-2Ag later at 3 months (50).

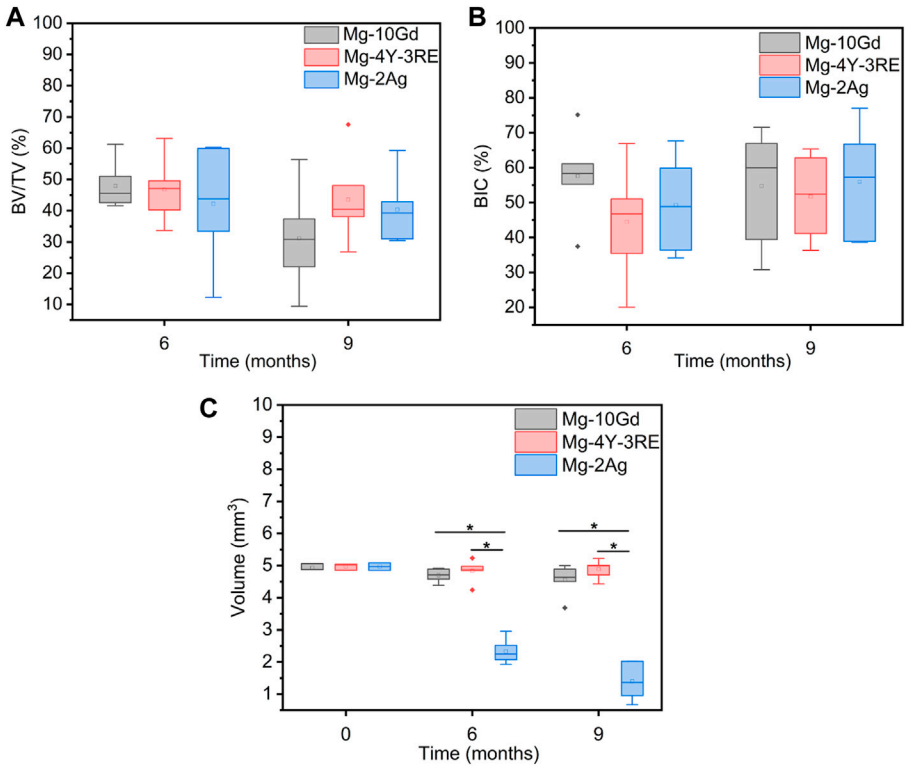

FIGURE 6
Box plots of the results of **(A)** bone volume fraction (BV/TV), **(B)** bone implant contact (BIC) and **(C)** volume of the screws calculated from the tomograms. The initial screw volumes are at time point = 0. The median is represented by a horizontal line in the box. The mean is represented by a small box within each boxplot. The whiskers correspond to the range. * means the result is significant. Number *n* = 36; test: one-way ANOVA.

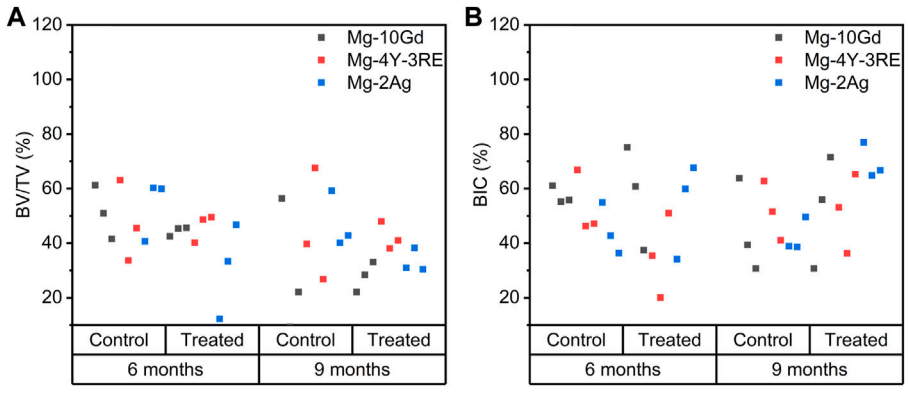

FIGURE 7
Scatter plots of the results of blood pre-incubation of the screws on Bone volume fraction (BV/TV) **(A)** and Bone implant contact (BIC) **(B)** between blood pre-incubated and control group of each material at 6 and 9 months.

On the contrary, in our current studies that focused on the long-term evaluation, the bone around the Mg-2Ag displayed matured morphology like the bone surrounding Mg-10Gd and Mg-4Y-3RE screws. This implies that, the screw types induced a similar osteogenic effect on the bone in the long term. For all screw types, the BIC recorded was above 40%, with Mg-2Ag and Mg-4Y-3RE screws showing slightly higher values at 9 months than 6 months. This indicates that the screws were anchored in the bone despite the occurrence of degradation. However, Mg-10Gd had a slightly reduced BIC at 9 months compared to 6 months but it is not enough grounds to conclude that BIC is compromised especially because of the observed intimate contact between the Mg-10Gd screws and the bone at both healing times (Figures 2, 4). It is worthwhile to point out that the osteotomy gap was completely bridged already at 6 months indicating that the screws were well encapsulated in the surrounding bone. A similar observation was reported by Krüger *et al.* at 3 months where Mg-5Gd and Mg-10Gd implants were well anchored in their surrounding bone without any gap between the implants and the bone at the bone implant interface compared to PEEK implants (30). This shows that improvement of osseointegration can be achieved with Mg-based implants. Remarkably, in our investigation, the disintegration of Mg-2Ag upon degradation did not compromise the bonding with the surrounding bone although it seems its mechanical competence could be compromised due to the severity of the degradation. A contradictory observation was reported by Galli et al. where already at 3 months, BIC among Mg-2Ag screws was sparsely in contact with bone with an average value below 10% (50). We can hypothesize that at the shorter healing times of 1 and 3 months faster changes were occurring in the degrading Mg-2Ag screws, not allowing a stable interface for the bone to be deposited and mature in contact with these screws. At the longer healing times we observed, the formation of more stable degradation layers which probably constituted an anchorage for bone formation and maturation. Our results indicate that Mg-2Ag was per se non toxic for the bone, but was probably its degradation modality that was not beneficial for initial bone integration. However, their findings on Mg-10Gd and Mg-4Y-3RE align with the current study where the screws were well integrated in the surrounding bone.

Galli et al. also reported highest *in vivo* degradation rate for Mg-10Gd (1.15 ± 0.19 mm/year) followed by Mg-2Ag (1.01 ± 0.11 mm/year) and lastly Mg-4Y-3RE (0.82 ± 0.10 mm/year) at 1 month observation period (50). As stated earlier, the degradation rate could not be calculated in the current study due to the similar density between the degradation layer and residual screw. Calculating the degradation rate from µXRF maps would be erroneous due to the inhomogeneity in the degradation layer. However, a qualitative evaluation of the degradation profiles of the screw types could be made based on the appearances and volumes of their remnant screws at both implantation times (Figures 2–4). It may be hypothesized that Mg-10Gd and Mg-4Y-3RE degraded similarly because they exhibited similar morphology of the remnant screw where the original screw shapes were maintained with comparable remnant screw volumes at 6 and 9 months implantation times (Figures 2, 3). On the other hand, for Mg-2Ag, the shape of the remnant screws were considerably altered (Figures 2–4) and the remnant screw volumes at 6 and 9 months were significantly lower compared to Mg-10Gd and Mg-4Y-3RE screws (Figure 6). This could mean that Mg-2Ag degraded at a different rate in comparison to Mg-10Gd and Mg-4Y-3RE. The morphologies of the remnant screws presented in this study are consistent with the findings of Galli et al. (50), except that, in their study, the degradation layer of Mg-2Ag was loosely attached to fibrous tissue. The alteration in the appearance of Mg-2Ag could be attributed to its rapid degradation, which might have led to the formation of smaller degradation layer and more soluble degradation products in comparison to Mg-10Gd and Mg-4Y-3RE. This assumption is based on an earlier report by Zeller-Plumhoff et al. who reported that a fast degradation rate was associated with a lower precipitation rate (51). Conversely, Myrissa et al. recorded that Mg-10Gd degraded faster compared to pure Mg and Mg-2Ag *in vivo* at 4 weeks observation period (52). It is important to point out that the observations from the references (50) and (52) were focused on the early phase of implantation while our observations are focused on the late phase of implantation (6 and 9 months). Witte et al. also studied the differences in the degradation rate among different magnesium-based implants and concluded that when RE elements are added to Mg, the oxidation rate decreases, leading to a slower degradation (27) which aligns with the findings of the this study. The differences in reports between short-term and mid- term evaluations of Mg-based alloys reinforced the need for a long-term evaluation to obtain a better insight on the *in vivo* temporal performance of Mg-based implants.

By means of µXRF (Figure 5) we were able to qualitatively assess and visualize the distribution of the elements in the degradation layer, the surrounding bone and soft tissue after 9 months of implantation. Apart from the Gd, Y and Ag which are unique to each screw type based on the alloying elements, the constituent of the surrounding layer was detected as Ca and P similar for all screw types at 9 months implantation times. In Mg-4Y-3RE screws, the accumulation of Y only in the former implant area was apparent. No visible Y was seen in bone nor the surrounding soft tissue. On the other hand, Turyanskaya *et al.* detected notably pronounced spreading and accumulation of Y in the surrounding bone during the degradation of WZ21 implants at 1 month of implantation using µXRF technique (53). In an *in vitro* corrosion test of Mg-Y alloys, Y is said to be oxidized into yttrium oxide (Y_2O_3) upon migrating to the metal surface of the alloy which is suggestive of the accumulation of Y in the degradation layer (54). For Gd distribution, a recent study by Peruzzi *et al.* used neutron µCT to show that Gd remains localized in the degradation

layer following the degradation of Mg-5Gd and Mg-10Gd implants (55). Likewise, in the current study, we detected Gd accumulation only in the former implant area. No Gd signal was detected in the surrounding bone nor soft tissue. The situation is quite different in the Ag maps of Mg-2Ag samples. Although the Ag signal is only detected in the degradation layer, its morphology appears disintegrated. Therefore, it can be assumed that soluble Ag-complexes were formed upon degradation which then migrated and were either excreted or incorporated into the animal's metabolism. This assumption is based on the absence of Ag signal from the surrounding bone and soft tissue.

The decrease of Mg in the degradation layer is contrasted with a simultaneous elevation of Ca and P for all implant types which indicates that Mg is progressively substituted by P and Ca in the degradation layer. P and Ca are the two major constituents of hydroxyapatite ($Ca_{10}PO_4$ OH_2) which form the inorganic component of bone. Under physiological conditions, PO_4^{3-} and Ca^{2+} ions are known to precipitate on Mg-based implants *via* biomineralization processes (56). Thus, the presence of P and Ca in the degradation products of all implant types is indicative of the biocompatible effect of the investigated Mg-based screws. Also, the μXRF maps (Figure 5) confirm the presence of S in the degradation layers of all screw types and the surrounding bone and soft tissue which is indicative of the presence of proteins. For example, there is evidence of formation of Y-protein complexes after intravenous administration of Y (57). The signal intensity of S in Mg-2Ag appears brighter than that observed in Mg-10Gd and Mg-4Y-3RE degradation products which might mean that there is an occurrence of higher binding of proteins to Ag due its disintegration (48,49). Helmholz et al. also reported the formation of Ag-S agglomerates in the degradation layer of an *in vivo* study involving Mg-2Ag (58). From the histological slides (Figure 4), the evidence of formation protein complexes in the degradation layer of all screw types could also be ascertained. The degradation layer of Mg-10Gd and Mg-4Y-3RE both have similar purplish appearance which might indicate the similar staining of proteins by toluidine blue. The Y-precipitates of Mg-4Y-3RE screws seen in the SRμCT slides (Figure 2) can also be seen in the histological data (Figure 4). Conversely, the degradation layer of Mg-2Ag screws is brown in the histological data (Figure 4) which coincides with the high signal intensity of their corresponding S maps. This observation might support the notion of higher protein binding in the degradation layer of Mg-2Ag.

We also investigated the effect of blood pre-incubation of the three Mg alloys (Mg-10Gd, Mg-4Y-3RE and Mg-2Ag) on their *in vivo* biocompatibility against the control group of the respective alloys. We have recorded lower mean BV/TV (Figure 7A) in the blood pre-incubated group compared to the control group of all screw types at both 6 and 9 months implantation time. Notably, at 6 months, the lower mean BV/TV of blood pre-incubated Mg-2Ag group compared to the control group was significant ($p < 0.05$). At 6 and 9 months, the blood pre-incubated group had higher mean BIC compared to the control group of all screw types except Mg-4Y-3RE (Figure 6B). The higher mean BIC of Mg-2Ag blood pre-incubated group compared to the control group was significant ($p < 0.05$) at 9 months. As previously stated, proteins get adsorbed on the surfaces of biomaterials upon contact with blood (17) which then affect the biological response and the biocompatibility of the material (19). For Mg alloys, adsorbed proteins are known to improve their corrosion resistance and cell adhesion (15,21,25). There is evidence that adsorbed proteins on biomaterials can undergo changes in their conformational structures over time which in turn impacts the biomaterials through the modulation of cell behavior (59,60). A recent study by Romero-Givalan et al. also confirmed that adsorbed proteins undergo changes over time (18). Therefore, it can be assumed that the adsorbed protein layer on the screws also underwent structural changes, in the long-term. Also, the probable interaction between Mg ions and the protein layer cannot be undermined. It can further be assumed that the reduction in the Mg content over time following degradation of the screws might have modified the adsorption kinetics to favor cell attachment. Protein adsorption to a material can be done with either a single protein such as bovine serum albumin (BSA) or with a multiprotein solution such a blood plasma. *In vitro* results are mostly based on single proteins, therefore, do not fully approximate the reaction observed for implanted biomaterials. It is also worthwhile to mention that surfaces vary in the selectivity of adsorption and the biological activity of the adsorbed proteins also varies among different surfaces, which accounts for the variable results among the screw types.

While our study successfully evaluated the long-term *in vivo* behavior, the distribution of degradation products as well as the influence of blood pre-incubation on three Mg-based alloys (Mg-10Gd, Mg-4Y-3RE and Mg-2Ag), a few open questions still exist. The time points in this study were limited to 6 and 9 months post implantation. Although we have shown in this study that, Y and Gd accumulate in the degradation layer, it is not clear how and for how long these degradation products remain in the degradation layer. Therefore future scope for biodegradable Mg implants research should focus on longer implantation times to monitor the evolution of the degradation products. This will give more understanding of whether the Gd and Y accumulations are permanent. A qualitative evaluation of the constituents of the degradation products was done in the current study. It would be worthwhile for future studies to quantitatively evaluate the long-term osseointegration of Mg degradation products to give an in-depth insight on the turn over of the degradation products. The current study offered valuable information on the long-term *in vivo* behavior of Mg-alloys, which is indispensable regarding alloy selection in biodegradable Mg-based implant development pathway.

5 Conclusion

In this study, the long-term effect of three different types of Mg-based alloys on bone were investigated using SRμCT, histology, and

μXRF. Utilizing the combination of these analytical methods we conclude that Mg-10Gd, Mg-4Y-3RE and Mg-2Ag exhibited a similar long-term osteogenic response since there was no statistically significant difference between the BV/TV and BIC among the explants at 6 and 9 months. The alloy with the lowest overall remnant screw volume was Mg-2Ag at both 6 and 9 months, which might signify fast degradability and a possible impairment in its mechanical properties. Blood pre-incubation significantly improved BIC in Mg-2Ag screw at 9 months but significantly retained lower BV/TV compared to the control at 6 months. We have successfully demonstrated that Mg-10Gd, Mg-4Y-3RE and Mg-2Ag promote osseointegration in the long-term with a similar bone response based on our quantified parameters. However, Mg-2Ag presented a different degradation dynamic from that of Mg-10Gd and Mg-4Y-3RE. The latter two alloys show the formation of insoluble degradation products preserving the shape of the initial implant. In contrast, Mg-2Ag shows a stronger reduction in the screws shape and fewer degradation products which might implicate less stable degradation products. Thus, we have consequently shown that short-term and mid-term *in vivo* investigations do not fully represent the complete degradation performance during the lifetime of such implants. Comparing our previous short and mid-term studies with our current long-term study, we have shown that these Mg alloys degrade in the long run into products that are very well tolerated by the body, hence they osseointegrate. Unfortunately, Mg-2Ag does that by going through an intense modification at the beginning, which makes it not very suitable for certain applications. Mg-10Gd and Mg-4Y-3RE corroded at a similar rate than Mg-2Ag and forms stable solid products, thus they osseointegrate well already at short time, while Mg-2Ag corrodes into products that are less stable, and cause fibrous reaction at first, then it stabilizes, because probably the degradation layer become more apatite-like, and at that point it osseointegrates. Furthermore, the RE elements Gd and Y used in the alloys remained at the implantation site. This finding could possibly imply that Gd and Y probably remained in the degradation layers, either in the apatite-like structure or in other solid by-products of the degradation. In the situation we have followed so far, up to 9 months, they did not show to induce local or systemic toxicity based on our qualitative evaluations. However, their prolonged presence in the degradation layers might implicate that these elements could be released later on, if the degradation layers of the Mg alloys will be further dissolved at later stages or they might persist in the implantation site forever. In general, these elements if not in the form of ions have not shown toxicity effect, but we cannot exclude that they will be released in the ionic form at later stages, and thus they could still pose toxicity risk in the future. Future scope for biodegradable Mg implants research should focus on even longer implantation times to better understand the evolution of the degradation products, their local and systemic effects as well as their mechanical integrity. Also, as adsorbed proteins undergo conformational changes over time, future studies should focus on comparatively investigating the early conformation of proteins adsorption on Mg alloys *in vivo* in short, mid and long-term studies as well as their effect on the degradation of Mg alloys.

Data availability statement

The raw data supporting the conclusions of this article will be made available by the authors, without undue reservation.

Ethics statement

The animal study was reviewed and approved by French Ministry of Higher Education and Research (approval number 00391-01).

Author contributions

SS: Formal analysis and Manuscript writing. DW: Conceptualization, Project administration and Formal Analysis. HH: Project administration and Formal analysis. BZ-P: Project administration and Formal analysis. AW: Project Administration. JM: Formal analysis. RW-R: Conceptualization. SG: Conceptualization, Project administration and Formal analysis.

Funding

This work was supported by the Röntgen-Angström Cluster in project Synchroload (05K16CGA), Swedish Research Council 2015-06109, the German Bundesminiterium für Bildung und Forschung in project MgBone (05K16CGB) and the People Programme (Marie Curie Actions) of the European Union's Seventh Framework Programme FP7/2007-2013/under REA grant agreement n289163.

Acknowledgments

We acknowledge the beamline P05, PETRA III, DESY, Germany, including the technical staff for support during beamtimes. We would like to acknowledge the Maxwell Computational Resources Operated at DESY. We also thank Ryo Jimbo, Yohei Jinno and Naito for surgical operations. We acknowledge Björn Wiese and Monika Luczak for material processing.

Conflict of interest

The authors declare that the research was conducted in the absence of any commercial or financial relationships that could be construed as a potential conflict of interest.

Publisher's note

References

1. Castellani C, Lindtner RA, Hausbrandt P, Tschegg E, Stanzl-Tschegg SE, Zanoni G, et al. (2011). Bone-implant interface strength and osseointegration: Biodegradable magnesium alloy versus standard titanium control. *Acta Biomater* 7 (1), 432–40. doi:10.1016/j.actbio.2010.08.020

2. Kaya AA (2020). A Review on Developments in Magnesium Alloys. *Frontiers in Materials* 7, 198. doi:10.3389/fmats.2020.00198

3. Bian D, Deng J, Li N, Chu X, Liu Y, Li W, et al. (2018). *In Vitro* and *in Vivo* Studies on Biomedical Magnesium Low-Alloying with Elements Gadolinium and Zinc for Orthopedic Implant Applications. *ACS Appl. Mater. Interfaces* 10 (5), 4394–408. doi:10.1021/acsami.7b15498

4. Tsakiris V, Tardei C, Clicinschi FM (2021). Biodegradable Mg alloys for orthopedic implants – A review. *Journal of Magnesium and Alloys* 9, 1884–905. doi:10.1016/j.jma.2021.06.024

5. Shikinami Y, Okuno M (1999 May 1). Bioresorbable devices made of forged composites of hydroxyapatite (HA) particles and poly-L-lactide (PLLA): Part I. Basic characteristics. *Biomaterials* 20 (9), 859–77. doi:10.1016/s0142-9612(98)00241-5

6. Jahnen-Dechent W, Ketteler M (2012). Magnesium basics. *Clin. Kidney J.* 2012 (5), 3–i14. doi:10.1093/ndtplus/sfr163

7. Al Alawi AM, Al Badi A, Al Huraizi A, Falhammar H (2021). Magnesium: The recent research and developments. *Advances in Food and Nutrition Research* 96, 193–218. doi:10.1016/bs.afnr.2021.01.001

8. Matsui M, Kuwata H, Yamauchi M, Gao P, Wu H, et al. (2009). Biodegradable surgical implants based on magnesium alloys – A review of current research. *IOP Conf Ser Mater Sci Eng* 4 (1), 012011. doi:10.1088/1757-899X/4/1/012011

9. Amukarimi S, Mozafari M (2022). Biodegradable Magnesium Biomaterials—Road to the Clinic. *Bioengineering (Basel).* 9 (3), 107. doi:10.3390/bioengineering9030107

10. Antoniac I, Adam R, Biță A, Miculescu M, Trante O, Petrescu IM, et al. (2021). Comparative assessment of *in vitro* and *in vivo* biodegradation of Mg-1Ca magnesium alloys for orthopedic applications. *Materials (Basel)* 14 (1), 84–20. doi:10.3390/ma14010084

11. Brar HS, Platt MO, Sarntinoranont M, Martin PI, Manuel M V (2009). Magnesium as a biodegradable and bioabsorbable material for medical implants. *JOM* 61, 31–34. doi:10.1007/s11837-009-0129-0

12. Witte F, Hort N, Vogt C, Cohen S, Kainer KU, Willumeit R, et al. (2008). Degradable biomaterials based on magnesium corrosion. *Curr. Opin. Solid State Mater. Sci.* 12 (5–6), 63–72. doi:10.1016/j.cossms.2009.04.001

13. Galli S (2016). On magnesium-containing implants for bone applications. Malmö University, Faculty of Odontology. (Doctoral Dissertation in Odontology).

14. Bowen PK, Drelich J, Goldman J (2014). Magnesium in the murine artery: probing the products of corrosion. *Acta Biomater* 10 (3), 1475–83. doi:10.1016/j.actbio.2013.11.021

15. Willumeit R, Möhring A, Feyerabend F (2014). Optimization of Cell Adhesion on Mg Based Implant Materials by Pre-Incubation under Cell Culture Conditions. *Int. J. Mol. Sci.* 15, 7639–7650. doi:10.3390/ijms15057639

16. Zhang ZQ, Wang HY, Wang L, Chen XB, Guan SK, Lin CG, et al. (2021). Protein conformation and electric attraction adsorption mechanisms on anodized magnesium alloy by molecular dynamics simulations. *J Magnes Alloy*. doi:10.1016/j.jma.2021.04.005

17. Kim J (2020 Apr 1). Systematic approach to characterize the dynamics of protein adsorption on the surface of biomaterials using proteomics. *Colloids and Surfaces B: Biointerfaces* 188, 110756. doi:10.1016/j.colsurfb.2019.110756

18. Romero-Gavilán F, Cerqueira A, Eduardo A, Tejero R, García-Arnáez I, Martinez-Ramos C, et al. (2021). Protein adsorption/desorption dynamics on Ca-enriched titanium surfaces: biological implications. *J. Biol. Inorg. Chem.* 26 (3), 715–26. doi:10.1007/s00775-021-01886-4

19. Romero-Gavilan F, Sánchez-Pérez AM, Araújo-Gomes N, Azkargorta M, Iloro I, Elortza F, et al. (2017). Proteomic analysis of silica hybrid sol-gel coatings: a potential tool for predicting the biocompatibility of implants *in vivo*. *Biofouling* 33 (8), 676–89. doi:10.1080/08927014.2017.1356289

20. Hiraguchi Y, Nagahashi K, Shibayama T, Hayashi T, Yano TA, Kushiro K, et al. (2014 Jul 1). Effect of the distribution of adsorbed proteins on cellular adhesion behaviors using surfaces of nanoscale phase-reversed amphiphilic block copolymers. *Acta Biomater.* 10 (7), 2988–95. doi:10.1016/j.actbio.2014.03.019

21. Rettig R, Virtanen S (2008). Time-dependent electrochemical characterization of the corrosion of a magnesium rare-earth alloy in simulated body fluids. *J. Biomed. Mater. Res. A* 85A, 167–175. doi:10.1002/jbm.a.31550

22. Yamamoto A, Hiromoto S (2009 Jun 1). Effect of inorganic salts, amino acids and proteins on the degradation of pure magnesium *in vitro*. *Materials Science and Engineering: C* 29 (5), 1559–68. doi:10.1016/j.msec.2008.12.015

23. Liu C, Xin Y, Tian X, Chu PK (2007). Degradation susceptibility of surgical magnesium alloy in artificial biological fluid containing albumin. *J. Mater. Res* 22, 1806–1814. doi:10.1557/jmr.2007.0241

24. Höhn S, Virtanen S, Boccaccini AR (2019 Jan 15). Protein adsorption on magnesium and its alloys: A review. *Appl. Surf. Sci.* 464, 212–9. doi:10.1016/j.apsusc.2018.08.173

25. Willumeit R, Wendel HP, Mihailova B, Feyerabend F (2014). How does blood contact change Magnesium degradation? European Cells and materials 28 (3), 29. Available from: https://www.researchgate.net/publication/269166868.

27. Witte F, Kaese V, Haferkamp H, Switzer E, Meyer-Lindenberg A, Wirth CJ, et al. (2005). *In vivo* corrosion of four magnesium alloys and the associated bone response. *Biomaterials* 26 (17), 3557–63. doi:10.1016/j.biomaterials.2004.09.049

28. Jähn K, Saito H, Taipaleenmäki H, Gasser A, Hort N, Feyerabend F, et al. (2016). Intramedullary Mg2Ag nails augment callus formation during fracture healing in mice. *Acta Biomater.* 36, 350–60. doi:10.1016/j.actbio.2016.03.041

29. Tie D, Feyerabend F, Müller W-D, Schade R, Liefeith K, Kainer K, et al. (2013). Antibacterial biodegradable Mg-Ag alloys. *Eur Cell Mate* 25, 284–98. doi:10.22203/ecm.v025a20

30. Krüger D, Galli S, Zeller-Plumhoff B, Wieland DCF, Peruzzi N, Wiese B, et al. (2021 Nov 14). High-resolution *ex vivo* analysis of the degradation and osseointegration of Mg-xGd implant screws in 3D. *Bioact. Mater.* 13, 37–52. doi:10.1016/j.bioactmat.2021.10.041

31. Myrissa A, Braeuer S, Martinelli E, Willumeit-Römer R, Goessler W, Weinberg AM (2017). Gadolinium accumulation in organs of Sprague–Dawley® rats after implantation of a biodegradable magnesium-gadolinium alloy. *Acta Biomater.* 48, 521–9. doi:10.1016/j.actbio.2016.11.024

32. Bruce DW, Hietbrink BE, DuBois KP (1963 Nov 1). The acute mammalian toxicity of rare earth nitrates and oxides. *Toxicol. Appl. Pharmacol.* 5 (6), 750–9. doi:10.1016/0041-008x(63)90067-x

33. Feyerabend F, Fischer J, Holtz J, Witte F, Willumeit R, Drücker H, et al. (2010). Evaluation of short-term effects of rare earth and other elements used in magnesium alloys on primary cells and cell lines. *Acta Biomater* 6 (5), 1834–42. doi:10.1016/j.actbio.2009.09.024

34. Cecchinato F, Agha NA, Martinez-Sanchez AH, Luthringer BJC, Feyerabend F, Jimbo R, et al. (2015). Influence of Magnesium Alloy Degradation on Undifferentiated Human Cells. *PLoS One* 10 (11), e0142117. doi:10.1371/journal.pone.0142117

35. Calado LM, Carmezim MJ, Montemor MF (2022). Rare Earth Based Magnesium Alloys—A Review on WE Series. *Frontiers in Materials* 8, 804906. doi:10.3389/fmats.2021.804906

36. Windhagen H, Radtke K, Weizbauer A, Diekmann J, Noll Y, Kreimeyer U, et al. (2013). Biodegradable magnesium-based screw clinically equivalent to titanium screw in hallux valgus surgery: short term results of the first prospective, randomized, controlled clinical pilot study. *Biomed Eng* 12 (1), 62. doi:10.1186/1475-925X-12-62

37. Zeller-Plumhoff B, Tolnai D, Wolff M, Greving I, Hort N, Willumeit-Römer R (2021). Utilizing Synchrotron Radiation for the Characterization of Biodegradable Magnesium Alloys—From Alloy Development to the Application as Implant. *Material. Adv Eng Mater* 23 (11), 2100197. doi:10.1002/adem.202100197

38. Schindelin J, Arganda-Carreras I, Frise E, Kaynig V, Longair M, Pietzsch T, et al. (2012). Fiji: an open-source platform for biological-image analysis. *Nat. Methods* 97, 676–682. doi:10.1038/nmeth.2019

39. Rueden CT, Schindelin J, Hiner MC, DeZonia BE, Walter AE, Arena ET, et al. (2017). ImageJ2: ImageJ for the next generation of scientific image data. *BMC Bioinformatics* 18, 529. doi:10.1186/s12859-017-1934-z

40. Wilde F, Ogurreck M, Greving I, Hammel JU, Beckmann F, Hipp A, et al. (2016). Micro-CT at the imaging beamline P05 at PETRA III. *AIP Conf. Proc.* 1741, 30035. doi:10.1063/1.4952858

41. Ogurreck M, Wilde F, Herzen J, Beckmann F, Nazmov V, Mohr J, et al. (2013). The nanotomography endstation at the PETRA III imaging beamline. *J. Phys, Conf. Ser.* 425 (18), 182002. doi:10.1088/1742-6596/425/18/182002

42. Haibel A, Ogurreck M, Beckmann F, Dose T, Wilde F, Herzen J, et al. (2010). Micro- and nano-tomography at the GKSS Imaging Beamline at PETRA III. *Dev X-Ray Tomogr VII* 7804, 78040B. doi:10.1117/12.860852

43. Haibel A, Beckmann F, Dose T, Herzen J, Ogurreck M, Müller M, et al. (2010). Latest developments in microtomography and nanotomography at PETRA III. *Powder Diffr* 25 (2), 161–4. doi:10.1154/1.3428364

44. Moosmann J, Ershov A, Weinhardt V, Baumbach T, Prasad MS, Labonne C, et al. (2014 92). Time-lapse X-ray phase-contrast microtomography for *in vivo* imaging and analysis of morphogenesis. *Nat. Protoc.* 9, 294–304. doi:10.1038/nprot.2014.033

45. Bruns S, Stipp SLS, Sørensen HO, Bruns S, Stipp SLS, Sørensen HO (2017). Looking for the Signal: A guide to iterative noise and artefact removal in X-ray tomographic reconstructions of porous geomaterials. *AdWR* 105, 96–107. doi:10.1016/j.advwatres.2017.04.020

46. Krüger D, Zeller-Plumhoff B, Wiese B, Yi S, Zuber M, Wieland DCF, et al. (2021). Assessing the microstructure and *in vitro* degradation behavior of Mg-xGd screw implants using µCT. *J Magnes Alloy* 9, 2207–2222. doi:10.1016/j.jma.2021.07.029

47. Donath K (1993). Preparation of histologic sections by cutting-grinding technique for hard tissue and other materials not suitable to be sectioned by routine methods. Available from: https://www.scienceopen.com/document?vid=9ee37648-854b-46e7-aee8-548e2de5877e.

48. Wang X, Herting G, Odnevall Wallinder I, Blomberg E (2015 Jul 28). Adsorption of bovine serum albumin on silver surfaces enhances the release of silver at pH neutral conditions. *Phys. Chem. Chem. Phys.* 17 (28), 18524–34. doi:10.1039/c5cp02306h

49. Wang C, Zanna S, Frateur I, Despax B, Raynaud P, Mercier-Bonin M, et al. (2016). BSA adsorption on a plasma-deposited silver nanocomposite film controls silver release: A QCM and XPS-based modelling. *Surf Coatings Technol* 307, 1–8. doi:10.1016/j.surfcoat.2016.07.063

50. Galli S, Hammel J, Agha N, Szakács G, Marco I, Lukac F, et al. (2016). Degradation behaviour and bone response of 3 magnesium alloys in comparison with titanium : An *in vivo* investigation.

51. Zeller-Plumhoff B, Gile M, Priebe M, Slominska H, Boll B, Wiese B, et al. (2021). Exploring key ionic interactions for magnesium degradation in simulated body fluid – A data-driven approach. *Corros Sci* 182, 109272. doi:10.1016/j.corsci.2021.109272

52. Myrissa A, Agha NA, Lu Y, Martinelli E, Eichler J, Szakács G, et al. (2016). *In vitro* and *in vivo* comparison of binary Mg alloys and pure Mg. *Mater Sci Eng C* 61, 865–74. doi:10.1016/j.msec.2015.12.064

53. Turyanskaya A, Rauwolf M, Grünewald TA, Meischel M, Stanzl-Tschegg S, Löffler JF, et al. (2016). µXRF Elemental Mapping of Bioresorbable Magnesium-Based Implants in Bone. *Materials* 9, 811. doi:10.3390/ma9100811

54. Johnson I, Liu H (2013). A study on factors affecting the degradation of magnesium and a magnesium-yttrium alloy for biomedical applications. *PLoS One* 8 (6), e65603. doi:10.1371/journal.pone.0065603

55. Peruzzi N, Galli S, Helmholz H, Kardjilov N, Krüger D, Markötter H, et al. (2021). Multimodal *ex vivo* methods reveal that Gd-rich corrosion byproducts remain at the implant site of biodegradable Mg-Gd screws. *Acta Biomater* 136, 582–91. doi:10.1016/j.actbio.2021.09.047

56. Zeller-Plumhoff B, Malich C, Krüger D, Campbell G, Wiese B, Galli S, et al. (2020 Jan 1). Analysis of the bone ultrastructure around biodegradable Mg–xGd implants using small angle X-ray scattering and X-ray diffraction. *Acta Biomater.* 101, 637–45. doi:10.1016/j.actbio.2019.11.030

57. Seitz JM, Eifler R, Bach FW, Maier HJ (2014). Magnesium degradation products: effects on tissue and human metabolism. *J. Biomed. Mater. Res. A* 102, 3744–3753. doi:10.1002/jbm.a.35023

58. Helmholz H, Luthringer-Feyerabend BJC, Willumeit-Römer R (2019). Elemental mapping of biodegradable magnesium-based implants in bone and soft tissue by means of µ X-ray fluorescence analysis. *J. Anal. At. Spectrom.* 34, 356–365. doi:10.1039/c8ja00377g

59. Faulón Marruecos D, Schwartz DK, Kaar JL (2018 Nov 1). Impact of surface interactions on protein conformation. *Curr. Opin. Colloid Interface Sci.* 38, 45–55. doi:10.1016/j.cocis.2018.08.002

60. Satzer P, Svec F, Sekot G, Jungbauer A (2016). Protein adsorption onto nanoparticles induces conformational changes: Particle size dependency, kinetics, and mechanisms. *Eng Life Sci* 16 (3), 238–46. doi:10.1002/elsc.201500059